

# Intensified UV/TiO<sub>2</sub> Photocatalytic Treatment of Colored Wastewater: Acid Orange 10 Removal in Closed and Semi-Closed Reactors

Sarah Chaouchi\* and Salima Bendebane

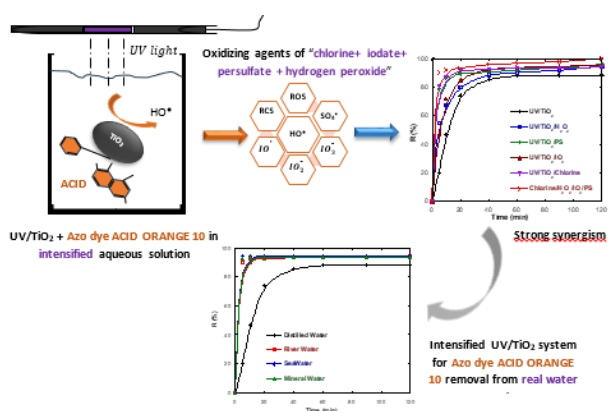
National Higher School of Technology and Engineering, Laboratory L3M, 23005, Annaba, Algeria

Received: 27/11/2025, Accepted: 20/01/2026, Available online: 21/01/2026

\*to whom all correspondence should be addressed: e-mail: s.chaouchi@ensti-annaba.dz

<https://doi.org/10.30955/gnj.08233>

## Graphical abstract



## Abstract

The treatment of wastewater containing synthetic dyes represents an environmental challenge due to their complex molecular structures and high stability. This study investigates the heterogeneous photocatalytic degradation of Acid Orange 10 (AO10), an azo dye widely used in the textile industry, using titanium dioxide (TiO<sub>2</sub>, Degussa P25) under ultraviolet (UV) irradiation in both closed and semi-closed photoreactor configurations.

Parametric optimization revealed that optimal degradation was achieved at pH 6.5, 25°C, and 0.1 g/L TiO<sub>2</sub> for an initial dye concentration of 10 mg/L, reaching 88% removal efficiency after 120 min in the UV/TiO<sub>2</sub> system.

Process intensification through the addition of oxidizing agents (H<sub>2</sub>O<sub>2</sub>, K<sub>2</sub>S<sub>2</sub>O<sub>8</sub>, Cl<sup>-</sup>, and IO<sub>3</sub><sup>-</sup>) significantly enhanced degradation performance. Among all tested systems, UV/TiO<sub>2</sub>/IO<sub>3</sub><sup>-</sup> exhibited the most remarkable enhancement, achieving 97% removal in 120 min, while the combined UV/TiO<sub>2</sub>/IO<sub>3</sub><sup>-</sup>/PS system achieved 97% removal in only 5 minutes, attributed to the synergistic generation of multiple reactive radicals (•OH, SO<sub>4</sub><sup>2-</sup>, and IO<sub>3</sub><sup>-</sup>).

Kinetic analysis confirmed that the degradation follows pseudo-first-order kinetics with excellent linearity ( $R^2 \geq$

0.99), with apparent rate constants increasing proportionally with oxidant addition.

Real matrix validation using river water, seawater, and mineral water confirmed the robustness of the process, maintaining >90% degradation efficiency despite the presence of interfering ions. These findings demonstrate that TiO<sub>2</sub>-based photocatalysis, intensified with oxidizing agents, represents an efficient and sustainable approach for treating dye-polluted effluents.

**Keywords:** TiO<sub>2</sub> photocatalysis; Acid Orange 10; Advanced Oxidation Processes; UV irradiation; Kinetics; Wastewater treatment.

## 1. Introduction

The global textile industry generates approximately 2.8 million tons of synthetic dyes annually, with an estimated 10-15% discharged into aquatic environments without adequate treatment (Kumar *et al.* 2023). Azo dyes, representing 60-70% of all textile dyes, exhibit particularly high persistence due to their stable -N=N- bonds (bond dissociation energy  $\approx$  250-270 kJ/mol), which resist conventional biological treatment methods that typically achieve only 10-30% color removal.

Synthetic dyes represent a major class of persistent organic pollutants, particularly in textile and paper factories. Their excessive release into aquatic environments cause severe ecological and health hazards due to the high toxicity, color persistence, and limited biodegradability (S. Abha *et al.* 2018, R. Ahmad *et al.* 2016). Among these, azo dyes are the largest group used with 60%-70% from the presented synthetic species in the textile industry (I. Oller *et al.* 2011).

The World Health Organization (WHO) estimates that approximately 80% of diseases in developing countries are waterborne, emphasizing the necessity of efficient wastewater purification (K. González-Labrada *et al.* 2020).

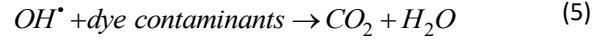
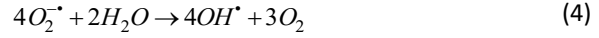
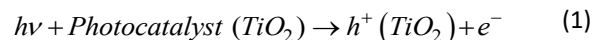
Conventional treatment techniques show limited effectiveness for azo dye removal. Biological degradation

methods typically achieve only 10-30% color removal due to the resistance of azo bonds to microbial oxidation (A. El-Ghemy et al. 2022). While adsorption methods can achieve higher removal efficiencies (60-90%), they merely transfer pollutants to another phase without destruction, generating secondary waste (saturated adsorbents) that requires disposal or regeneration. Coagulation-flocculation processes also suffer from incomplete color removal and sludge generation issues. These limitations underscore the need for destructive treatment methods such as advanced oxidation processes that achieve complete mineralization (H. Suty et al. 2021). AOPs rely on the generation of highly reactive oxidative species in sufficient amount, including hydroxyl radicals ( $\cdot\text{OH}$ ,  $E^\circ = 2.8$  eV) (H.J. Wang et al. 2025, M. Dai et al. 2024), oxygen atoms (L. Peng et al. 2024), oxygen molecules (Z. Zhu et al. 2022), which non-selectively drive the decomposition of organic pollutants into inoffensive byproducts,  $\text{CO}_2$ ,  $\text{H}_2\text{O}$ , and inorganic ions (H. Suty et al. 2021). photocatalytic oxidation classified as a cleaner and greener technology for azo dye degradation over the past decade (S. Li et al. 2023).

Advanced Oxidation Processes (AOPs), particularly photocatalysis, offer significant advantages over conventional methods for azo dye treatment. Unlike adsorption or coagulation, photocatalysis achieves complete mineralization rather than phase transfer, eliminating secondary waste generation. Compared to biological treatment, photocatalytic processes are not inhibited by toxic or recalcitrant compounds and operate effectively at high dye concentrations. Recent studies have demonstrated that photocatalytic systems achieve superior removal efficiencies (>90%) compared to biological treatment (10-30%), activated carbon adsorption (60-80%), and electrocoagulation (50-70%) for azo dyes (Yudha Gusti Wibowo et al. 2025). Furthermore, photocatalysis generates powerful oxidizing species ( $\cdot\text{OH}$ ,  $E^\circ = 2.8$  V) that non-selectively attack organic pollutants, ensuring complete degradation of complex aromatic structures. The process operates at ambient temperature and pressure, requires no chemical addition (beyond the recyclable photocatalyst), and can utilize solar energy, offering both environmental and economic advantages for sustainable wastewater treatment (A. Dari Jaafar et al. 2024)

Photocatalytic advanced oxidation processes (P-AOPs), particularly using  $\text{TiO}_2$  as a semiconductor catalyst with a wide band gap (3.2 eV), is one of the most promising AOPs due to its high photoactivity, low cost, and chemical stability (M.R. Hoffmann et al. 2022, M. Samadi et al. 2016).

The basic mechanism of photocatalytic starts with light absorption by the photocatalyst ( $\text{TiO}_2$  absorbs UV radiation < 380 nm), generating electron-hole pairs that initiate redox reactions. The adsorption of the dye compounds onto the photocatalyst surface on which oxidative processes occur, leading to pollutant mineralization (N. Guettai et al. 2005). The reactions responsible for the photocatalytic dye degradation can be summarized as follows:



Several studies have reported  $\text{TiO}_2/\text{UV}$  systems for dye degradation, yet their performance is limited by factors such as catalyst aggregation, electron-hole recombination, and incomplete mineralization (Y. Zhao et al. 2020, S. Karuppaiah et al. 2019). Photocatalytic process intensification involves strong oxidizing agents in addition to  $\cdot\text{OH}$ , such as persulfate, hydrogen peroxide, periodate and chlorine, can significantly improve efficiency by generating additional radicals (G. V. Buxton et al. 1985, F. Zaviska et al. 2003).

persulfate addition to photocatalysis can lead to the generation of sulfate radicals ( $\text{SO}_4^{\cdot-}$ ) (Q. Yang et al. 2019). The photoactivation of periodate generate iodate ions ( $\text{IO}_3^-$ ), hydrogen peroxide ( $\text{H}_2\text{O}_2$ ), oxygen ( $\text{O}_2$ ), and ozone ( $\text{O}_3$ ). In the same system, highly reactive brief radicals as iodyl ( $\text{IO}_3^\cdot$ ), periodyl ( $\text{IO}_4^\cdot$ ), hydroxyl ( $\cdot\text{OH}$ ), are also produced again enhancing the oxidation of azo dye (X. Zhang et al. 2021, M. L. Djaballah et al. 2021).

In the UV/chlorine oxidation process (at 254 nm irradiation), hydroxyl radicals and several varieties of oxidants called reactive chlorine species (RCS) could be created ( $\text{Cl}^\cdot$ ,  $\text{ClO}^\cdot$ , and  $\text{Cl}_2^\cdot$ ) (Z. Lu et al. 2022). These species are mainly responsible for the degradation of pollutants.

In addition, extra of  $\cdot\text{OH}$  can be formed too by directly photolysis of water using 185 nm radiation ( L. Furanian et al. 2018).

This work investigates the photocatalytic degradation of Acid Orange 10 (ACID ORANGE 10) under UV irradiation in closed and semi-closed reactors using  $\text{TiO}_2$  as a catalyst. The study systematically examines the effects of process variables (pH, temperature, catalyst loading, and initial concentration) and explores process intensification through oxidant addition. Kinetic modeling and experiments in real water matrices provide a comprehensive understanding of the system's performance and practical potential for wastewater treatment.

## 2. Materials and Methods

### 2.1. Chemicals and Solutions

All reagents were of analytical grade and used without further purification. **Acid Orange 10 (ACID ORANGE 10)** was selected as a model pollutant from Sigma-Aldrich, with CAS number: 1936-15-8, and purity:  $\geq 85\%$ . specification of the ACID ORANGE 10 is presented in **Table 1**.

**Table 1.** Specification of Acid Orange 10

Chemical name	Acid Orange 10
Molecular mass (g/mol)	452.36
Maximum absorption wavelength	475 nm
Molecular formula	<i>C<sub>16</sub>H<sub>10</sub>N<sub>2</sub>Na<sub>2</sub>O<sub>7</sub>S<sub>2</sub></i>
Chemical Structure	

The **photocatalyst** used was **titanium dioxide (TiO<sub>2</sub>, Degussa P25)**, from Evonik Industries. A white semiconductor powder with average primary particle size: 21 nm. TiO<sub>2</sub> composed of ~80% anatase and ~20% rutile, with a molecular mass of 79.87 g/mol, density of 4.23 g/cm, and melting point of 1843°C, BET (Brunauer–Emmett–Teller) surface area: 50 ± 15 m<sup>2</sup>/g, and Band gap: 3.2 eV.

The **oxidizing agents** included potassium persulfate (K<sub>2</sub>S<sub>2</sub>O<sub>8</sub>, Purity ≥99%, Sigma-Aldrich, CAS 7727-21-1), potassium iodate (KIO<sub>3</sub>, Purity ≥99%, Sigma-Aldrich, CAS 7758-05-6), hydrogen peroxide (H<sub>2</sub>O<sub>2</sub>, 30% solution, Merck, CAS 7722-84-1), sodium hypochlorite (NaClO, 13% active chlorine, VWR, CAS 7681-52-9), and other supporting salts (KH<sub>2</sub>PO<sub>4</sub>, K<sub>2</sub>SO<sub>4</sub>, KNO<sub>3</sub>, K<sub>2</sub>CrO<sub>4</sub>, K<sub>4</sub>[Fe(CN)<sub>6</sub>]-3H<sub>2</sub>O), with Purity ≥99%, Sigma-Aldrich.

Each oxidant was selected for its ability to generate radicals such as SO<sub>4</sub><sup>•-</sup>, OH<sup>•</sup>, IO<sup>•</sup>, or Cl<sup>•</sup> under UV excitation.

**Alcohols** (Ethanol C<sub>2</sub>H<sub>5</sub>OH: Purity ≥99.8%, absolute, Sigma-Aldrich, 2-Propanol C<sub>3</sub>H<sub>7</sub>OH: Purity ≥99.5%, Sigma-Aldrich, and tert-Butanol C<sub>4</sub>H<sub>9</sub>OH: Purity ≥99%, Sigma-Aldrich) were used as radical scavengers, while **Ascorbic acid** C<sub>6</sub>H<sub>8</sub>O<sub>6</sub>: Purity ≥99%, Sigma-Aldrich) served as a reducing agent in certain control tests.

All working solutions were freshly prepared in distilled water, with Conductivity <2 μS/cm, produced in-laboratory, and pH was adjusted to 6.5 ± 0.1 using 0.1 M of Sodium hydroxide (NaOH): Purity ≥98%, pellets, Merck, or Hydrochloric acid (HCl): 37%, Merck, using HANNA pH-211 meter, calibrated at pH 4, 7, and 10.

To ensure complete dispersion of the contaminants in the solution, the solution was mixed with the required amount of catalyst and magnetically spun in the dark. The UV light, located at the center of the reactor, was then turned on. An external water-cooling system was used around the reactor to maintain the temperature during the process experiments.

## 2.2. Photocatalytic Reactor (Closed System)

Photocatalytic experiments were conducted in a cylindrical borosilicate glass reactor with a total capacity of 500 mL and an effective working volume of 250 mL (Figure 1). The reactor had an internal diameter of 8 cm

and a height of 15 cm. Irradiation was provided by a low-pressure mercury UV lamp ( $\lambda = 254$  nm, 12 W), positioned vertically at a fixed distance of 5 cm above the liquid surface to ensure uniform photon distribution. The reactor was enclosed with an aluminum shield to minimize external light interference and enhance UV reflection toward the reaction medium. The reaction temperature was maintained at 25 ± 1°C, continuously monitored using a K-type thermocouple with an accuracy of ±0.5°C, immersed directly in the solution. The suspension was continuously agitated using a magnetic stirrer operating at 300 rpm, equipped with a 2 cm magnetic stir bar, to ensure homogeneous dispersion of TiO<sub>2</sub> particles throughout the reaction medium. The initial pH was adjusted to 6.5 and measured before and after each experiment using a combined glass electrode (HANNA pH-211).

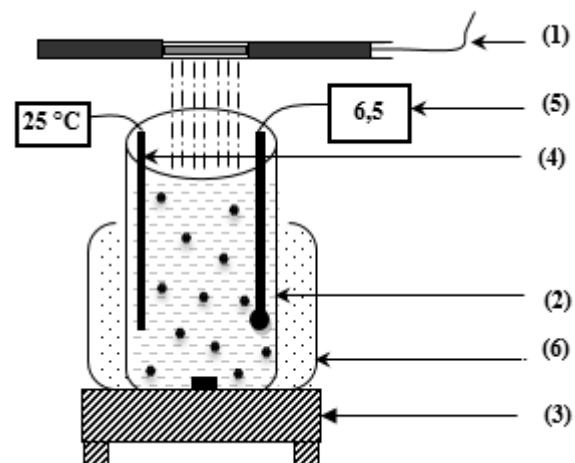


**Figure 1.** Experimental setup of the closed photocatalytic reactor. Components: (1) UV lamp 254 nm, 12 W, positioned 5 cm above liquid surface; (2) cylindrical borosilicate glass reactor ( $\varnothing = 8$  cm, H = 15 cm, V = 250 mL); (3) magnetic stirrer (300 rpm); (4) K-type thermocouple; (5) pH meter; (6) ultrasonic transducer (40 kHz, 100 W, positioned at external bottom—used only for experiments in Figure 5). Operational conditions: [AO10] = 10 mg/L, [TiO<sub>2</sub>] = 0.1 g/L, pH 6.5.

## 2.3. Semi-Closed Photocatalytic System

To enhance mass transfer and photon utilization efficiency, a semi-closed dual-reactor configuration was employed (Figure 2). The system consisted of two

identical cylindrical borosilicate glass reactors, each having the same dimensions as the closed system reactor (8 cm diameter and 15 cm height), and separated by a fixed distance of 50 cm. Both reactors were equipped with cooling jackets to maintain a constant operating temperature of 25°C. Continuous circulation of the ACID ORANGE 10 suspension between the two reactors was ensured by a peristaltic pump (Kerlabo) operating at a constant flow rate of 100 mL/min, maintaining a total working volume of 250 mL and a TiO<sub>2</sub> concentration of 0.1 g/L. The system was irradiated simultaneously using two UV sources: a low-pressure mercury lamp (254 nm) and a high-power UV lamp (UVITALux, 300 W, 280–400 nm, UV-A/B range). This configuration enabled sequential exposure of the circulating suspension to different UV intensities and spectral ranges, thereby improving photocatalytic efficiency. Experiments were conducted for 120 minutes, with periodic sampling for kinetic monitoring. **Figure 2.** Experimental setup of the semi-closed photocatalytic system with continuous circulation between two UV-irradiated reactors. After each irradiation interval, aliquots were withdrawn and centrifuged using a REMI R-8C DX centrifuge at 4500 rpm for 30 min at 25°C to remove suspended TiO<sub>2</sub> particles and avoid light scattering during UV-Vis analysis. This separation step ensured accurate determination of the residual dye concentration.

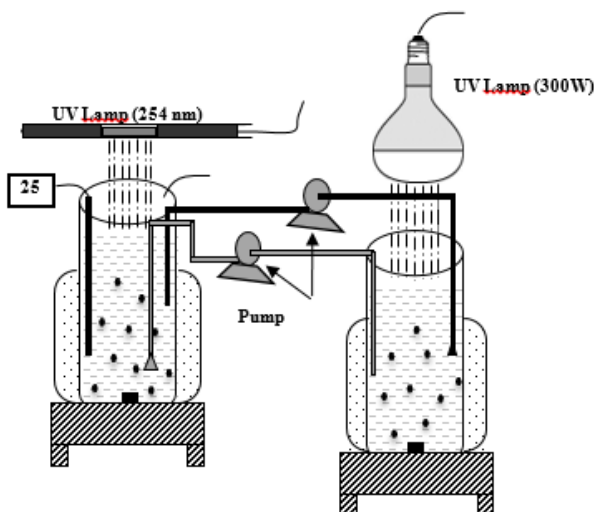


**Figure 2.** Experimental setup of the semi-closed photocatalytic system with continuous circulation between two UV-irradiated reactors.

#### 2.4. Spectrophotometric Analysis

The degradation of ACID ORANGE 10 was monitored by **UV-Vis spectrophotometry** using a **Shimadzu UV-1900i** spectrophotometer equipped with 1 cm quartz cells.

Absorbance was measured at  $\lambda_{\text{max}} = 482 \text{ nm}$ , corresponding to the characteristic band of the azo chromophore (–N=N–) of ACID ORANGE 10.

The concentration of the dye was determined using the **Beer-Lambert law**, and the degradation efficiency ( $\eta$ ) was calculated as:

$$\eta(\%) = \frac{C_0 - C_t}{C_0} \times 100 \quad (6)$$

Where:

$\eta$  = degradation efficiency (%)

$C_0$  = initial dye concentration (mg/L;  $C_t$  = dye concentration at time  $t$  (mg/L)

### 3. Results and Discussion

#### 3.1. Photocatalytic degradation in the closed reactor

##### 3.1.1. Adsorption on TiO<sub>2</sub>

For the catalytic reaction, surface area providing adsorption sites for the substrate, and the overall rate depending on surface reactions, the physical and structural properties of those catalysts. While, photocatalysts have their own activity.

To identify the optimal conditions for dye degradation by photocatalysis and to ensure that the observed ACID ORANGE 10 removal results from oxidation rather than simple physical adsorption onto the catalyst surface, preliminary adsorption tests were carried out on TiO<sub>2</sub>.

Initially, the adsorption of ACID ORANGE 10 onto titanium dioxide was investigated under dark conditions. A 250 mL solution containing 10 mg/L ACID ORANGE 10 and 0.1 g/L TiO<sub>2</sub> was magnetically stirred for one hour. The variation of the normalized concentration ( $C/C_0$ ) as a function of contact time with TiO<sub>2</sub> is presented in **Figure 3**.

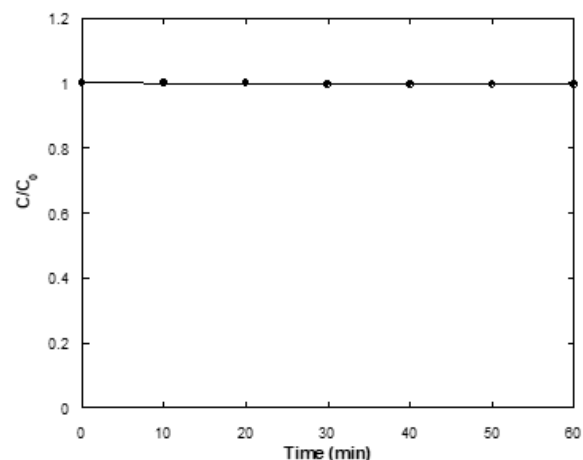


**Figure 3.** Adsorption kinetics of ACID ORANGE 10 on TiO<sub>2</sub> ([ACID ORANGE 10] = 10 mg/L; [TiO<sub>2</sub>] = 0.1 g/L; V = 250 mL; T = 25°C)

At the initial time ( $t = 0$ ),  $C/C_0 = 1.0$ , representing the starting condition. During the first 10 minutes of contact under dark conditions, the normalized concentration decreased from 1.0 to approximately 0.96, corresponding to 4% removal by physical adsorption onto the TiO<sub>2</sub> surface. After this initial period, the  $C/C_0$  value remained constant at approximately 0.96, indicating that adsorption equilibrium had been established. This equilibrium state persisted even after 60 minutes of continuous stirring, confirming that no additional adsorption occurred beyond the initial 10-minute period.

Increasing the TiO<sub>2</sub> mass does not necessarily lead to a higher number of adsorption sites or an improved adsorption rate (E. Vulliet *et al.* 2003). This behavior can be attributed to two major factors: (i) increasing the TiO<sub>2</sub> loading may induce pH variations in

the solution, thereby altering the surface charge state of the catalyst and reducing its affinity toward the dye molecules;

(ii) excessive TiO<sub>2</sub> concentrations promote particle agglomeration, which decreases the number of accessible active sites and consequently limits the adsorption efficiency (M. Sleiman *et al.* 2009, Y. Lin *et al.* 2009).

Previous studies have also shown that ACID ORANGE 10 exhibits weak adsorption on catalyst surfaces, with very similar adsorption constants, which explains the small amount adsorbed on TiO<sub>2</sub> and the consistently low adsorption capacities reported for similar system (R. Brina *et al.* 1987, X. Zhang *et al.* 2019) (Figure 4).

### 3.1.2. Direct photolysis

To assess the true efficiency of the photocatalytic process, it was essential to determine the contribution of direct photolysis to ACID ORANGE 10 degradation under the same operational conditions. For this purpose, a control experiment was conducted using a 10 mg/L ACID ORANGE 10 solution exposed to UV irradiation at 254 nm in the absence of TiO<sub>2</sub>.

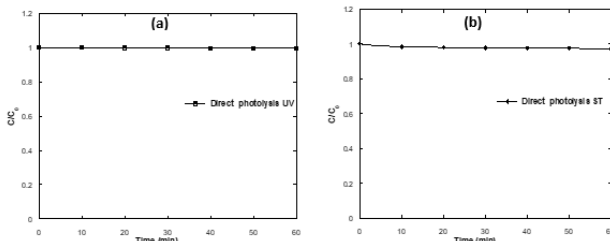


**Figure 4.** Presents the variation of the normalized concentration ( $C/C_0$ ) of ACID ORANGE 10 as a function of irradiation time under both UV (a) and simulated solar light (ST) (b). ( $[ACID\ ORANGE\ 10] = 10\ mg/L; V = 250\ mL; T = 25^\circ C$ )

The results clearly show that ACID ORANGE 10 solution has not undergone any change during these 60 min of direct photolysis. At the end, only a 2% decrease in concentration was observed, indicating that ACID ORANGE 10 is highly stable under UV light alone. UV-Vis spectral analysis confirmed that no significant change occurred in the absorption spectra throughout the experiment.

These findings confirm that any subsequent removal of ACID ORANGE 10 in the presence of TiO<sub>2</sub> results from true photocatalytic oxidation rather than direct photolysis, in agreement with previous studies on azo dyes under similar UV conditions (C. Lee *et al.* 2023, L. Zhang *et al.* 2024, J. Díaz-Torres *et al.* 2022).

### 3.1.3. Effect of different TiO<sub>2</sub> activation sources (UV, US, ST)

Photocatalytic dye removal inherently light-dependent. Under different light (UV, visible, and solar lights) irradiation, the penetration of light on TiO<sub>2</sub> particles generate electron-hole pairs, that enhances the production of reactive oxygen species, especially OH•, which plays a central role in dye mineralization.

Combination of ultrasonic (US) waves with heterogeneous catalysts is an important strategy that led to the increase

in photo-thermal catalytic activity, and controlling surface properties of catalysts (A. V. Mohod *et al.* 2023).

The activation of the TiO<sub>2</sub> semiconductor under various irradiation sources, including a 12 W UV-C lamp, a 300 W UV-A simulator lamp (ST), and ultrasonic activation (US) at low frequency were investigated. The corresponding degradation profiles of ACID ORANGE 10 are shown in Figure 5.

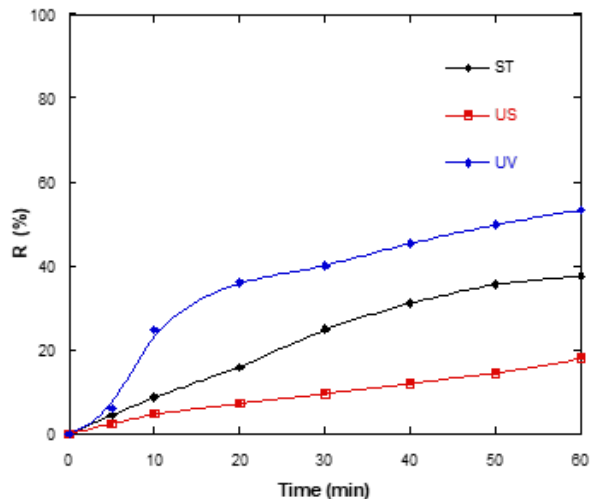


**Figure 5.** Degradation profiles of ACID ORANGE 10 ( $[ACID\ ORANGE\ 10] = 10\ mg/L; [TiO_2] = 0.1\ g/L; V = 250\ mL; T = 25^\circ C$ )

The results reveal a marked influence of the irradiation source on the photocatalytic performance. Under UV-C irradiation, ACID ORANGE 10 degradation reached 52% after 60 min, compared to 36% under simulated solar light and only 17% under ultrasonic activation.

The superior performance of UV activation is attributed to the higher photon energy ( $\lambda = 254\ nm$ ), which effectively excites the TiO<sub>2</sub> band gap (3.2 eV) and generates a larger number of electron-hole pairs.

The moderate activity under simulated solar light is associated with the limited fraction of photons in the UV range capable of initiating photocatalytic reactions. In contrast, ultrasonic activation induced only partial degradation, due to the low increased generation of electron-hole pairs and the limited production of hydroxyl radicals, whose contribution remained minor compared with direct UV photoexcitation (C. Lee *et al.* 2023, L. Zhang *et al.* 2024, J. Díaz-Torres *et al.* 2022).

poor light absorption, and relatively small specific surface area limited generation of reactive oxygen species (ROS) and therefore prevent its catalytic performance. These results highlight the critical role of photon energy in TiO<sub>2</sub> activation and confirm that UV-driven processes are far more efficient for the degradation of ACID ORANGE 10 and similar azo dyes.

### 3.1.4. Photocatalysis and degradation spectra

**Figure 6** shows the evolution of the UV-Vis absorption spectra of ACID ORANGE 10 during photocatalytic treatment under UV irradiation.

**Figure 6** displays the variations in the UV-visible spectrum of ACID ORANGE 10 dye solution over time. The dye's

characteristic wavelength, 482 nm, corresponding to the  $\pi-\pi^*$  transition of the azo ( $-N=N-$ ) chromophore. As the irradiation time increases, this band progressively decreases in intensity and nearly disappears after 120 minutes of photocatalysis.

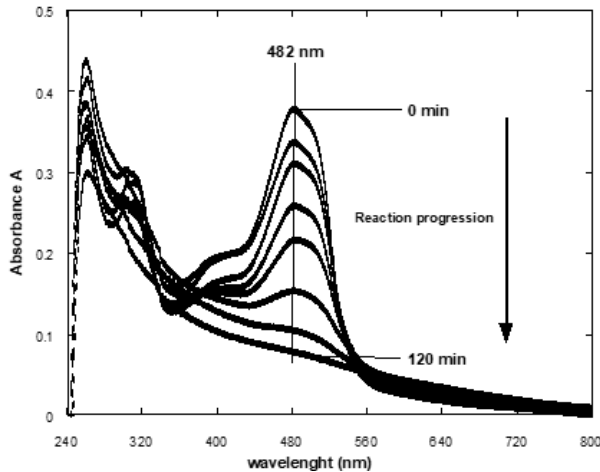


**Figure 6.** Evolution of the UV-Vis absorption spectra of Acid Orange 10 during photocatalytic treatment under UV irradiation in closed reactor configuration. Experimental conditions:  $[AO10]_0 = 10 \text{ mg/L}$ ;  $[\text{TiO}_2] = 0.1 \text{ g/L}$ ;  $\text{pH} = 6.5$ ;  $T = 25^\circ\text{C}$ ;  $V = 250 \text{ mL}$ ; UV lamp = 254 nm (12 W). Spectra recorded at 0, 15, 30, 60, 90, and 120 min.

The gradual decrease and eventual disappearance of the 482 nm band indicate the cleavage of the azo linkage and the breakdown of the conjugated aromatic structure of ACID ORANGE 10. These spectral changes confirm that the photocatalytic process effectively decomposes the chromophoric system into smaller, non-absorbing intermediates.

The broadening and slight shift in the spectra observed during degradation can be attributed to the formation of transient aromatic intermediates, which are subsequently mineralized into low-molecular-weight species. Similar spectral behavior has been reported for other azo dyes degraded by  $\text{TiO}_2$ -based photocatalysts (C. Lee *et al.* 2023, L. Zhang *et al.* 2024, J. Díaz-Torres *et al.* 2022).

### 3.2. Parametric study

#### 3.2.1. Effect of initial ACID ORANGE 10 concentration and kinetic analysis

The influence of the initial dye concentration on the photocatalytic degradation of ACID ORANGE 10 was examined in the range of 5-40 mg/L at natural pH and a constant  $\text{TiO}_2$  loading of 0.1 g/L.

As shown in **Figure 7**, the degradation rate decreased with increasing dye concentration under constant catalyst loading. At low concentrations ( $\leq 10 \text{ mg/L}$ ), almost complete elimination (88.31%) was achieved within 120 min, whereas higher concentrations resulted in slower degradation (76.27%). This behavior is attributed to photon screening as a result of the intensified concentration gradient, and the limited availability of active sites, has an inhibitory effect on the production of holes and OH radicals. Moreover, competitive reaction may occur between dye molecules and reactive species

generated during the degradation, which could potentially explain the observed decrease in degradation efficiency. Furthermore, the number of radicals generated through photocatalytic process becomes insufficient relatively to the increasing number of dye molecules.

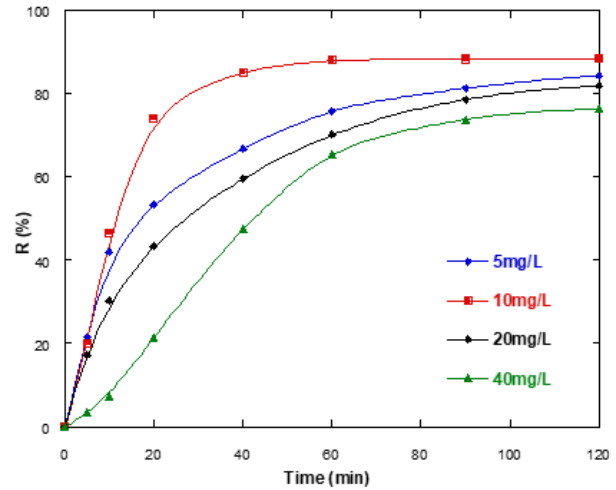


**Figure 7.** Effect of the initial ACID ORANGE 10 concentration ( $[\text{TiO}_2] = 0.1 \text{ g/L}$ ;  $V = 250 \text{ mL}$ ;  $T = 25^\circ\text{C}$ )

The kinetic behavior of ACID ORANGE 10 degradation was evaluated using the pseudo-first-order model:

$$r = -\frac{dC}{dt} = k_{app} C \quad (7)$$

$$\Rightarrow \ln \frac{C_0}{C} = k_{app} t \quad (8)$$

Where :

$r$  : rate of photocatalytic reaction

$C$  : dye concentration at time  $t$  (mg/L)

$C_0$  : initial dye concentration (mg/L)

$t$  : time (min)

$k_{app}$  : the apparent rate constant ( $\text{min}^{-1}$ )

The plots of  $\ln \frac{C_0}{C}$  versus irradiation time (**Figure 8**) exhibit excellent linearity ( $R^2 \geq 0.99$ ), confirming that ACID ORANGE 10 degradation follows pseudo-first-order kinetics.

The apparent rate constant ( $k_{app}$ ) decreases with increasing  $C_0$ , reflecting the combined effects of light attenuation and surface saturation. This trend is consistent with the Langmuir-Hinshelwood kinetic model commonly observed for  $\text{TiO}_2$  photocatalysis (C. Lee *et al.* 2023, L. Zhang *et al.* 2024, J. Díaz-Torres *et al.* 2022).

#### 3.2.2. Effect of $\text{TiO}_2$ Dosage

The influence of the catalyst mass on the photocatalytic degradation of ACID ORANGE 10 was investigated using different  $\text{TiO}_2$  dosages: 0.01, 0.05, 0.1, 0.5, and 1 g/L.

As shown in **Figure 9**, the degradation rate increases with  $\text{TiO}_2$  loading up to 0.1 g/L, beyond which the efficiency levels off. The initial rate enhancement is attributed to the larger surface area available for photon absorption and dye adsorption, resulting in the generation of more

electron-hole pairs and reactive hydroxyl radicals ( $\cdot\text{OH}$ ). Hence, the more active sites, the better the catalyst performance (A. Dari *et al.* 2025).

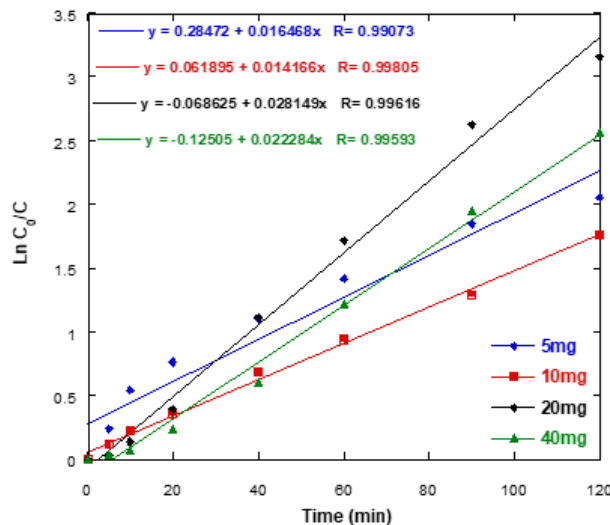


Figure 8. First-order reaction rate ( $[\text{TiO}_2] = 0.1 \text{ g L}^{-1}$ ;  $V = 250 \text{ mL}$ ;  $T = 25^\circ\text{C}$ )

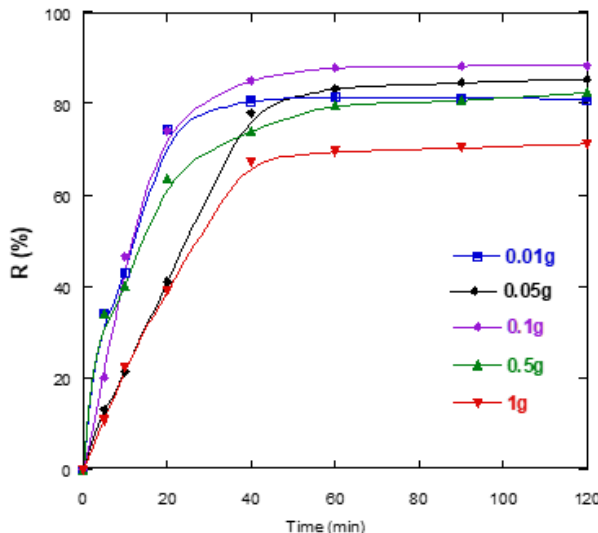


Figure 9. Effect of  $\text{TiO}_2$  mass on the photocatalytic degradation of ACID ORANGE 10 ( $[\text{ACID ORANGE 10}] = 10 \text{ mg L}^{-1}$ ;  $V = 250 \text{ mL}$ ;  $T = 25^\circ\text{C}$ )

However, when the  $\text{TiO}_2$  concentration exceeds  $0.1 \text{ g/L}$ , the reaction rate no longer improves significantly and even slightly decreases. This decline is due to light scattering and both of opacity and turbidity of the suspension at higher catalyst loadings, which reduce the effective photon flux reaching the catalyst surface. Moreover, excessive particle agglomeration at high concentrations can limit the number of available active sites and hinder the diffusion of dye molecules toward the surface (C. Lee *et al.* 2023, L. Zhang *et al.* 2024, J. Díaz-Torres *et al.* 2022).

Since surface area and particle size are closely related to each other, it can empirically be stated that the smaller the particle size is, the higher is the activity of a photocatalyst. The optimal  $\text{TiO}_2$  loading was therefore fixed at **0.1 g/L**, corresponding to a balance between efficient photon utilization and minimal light attenuation. Similar optimal values have been reported in the

photocatalytic degradation of other azo dyes and organic contaminants using Degussa P25  $\text{TiO}_2$  under comparable conditions (J. Díaz-Torres *et al.* 2022, M. R. Hoffmann *et al.* 2022, G. R. Peyton *et al.* 1974).

### 3.2.3. Effect of pH

The pH of the reaction medium is a crucial operational parameter in photocatalytic processes because it strongly influences the surface charge of  $\text{TiO}_2$  and the ionization state of the dye. The photocatalytic degradation of ACID ORANGE 10 was examined at different pH values (1, 3, 6.5, 9, and 12). The pH was adjusted using HCl for acidic and NaOH for basic conditions.

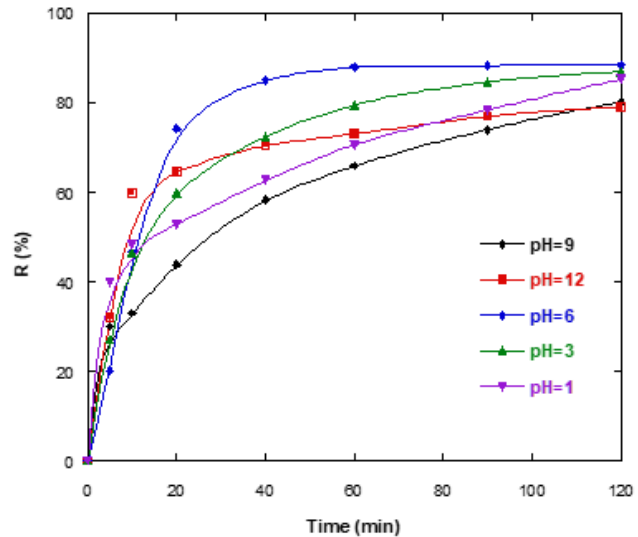


Figure 10. Effect of solution pH on the photocatalytic degradation of ACID ORANGE 10 ( $[\text{ACID ORANGE 10}] = 10 \text{ mg L}^{-1}$ ;  $[\text{TiO}_2] = 0.1 \text{ g L}^{-1}$ ;  $V = 250 \text{ mL}$ ;  $T = 25^\circ\text{C}$ )

As shown in Figure 10, the degradation rate was highest under mildly acidic conditions (pH 3-6), decreased at high pH, and was almost constant near neutral conditions. This behavior can be explained by electrostatic interactions between the charged  $\text{TiO}_2$  surface and the ionic dye species.  $\text{TiO}_2$  is amphoteric and exhibits a point of zero charge (PZC) around pH 6.8 (Degussa P25). When  $\text{pH} < \text{PZC}$ , the catalyst surface is positively charged, favoring adsorption of anionic dyes such as ACID ORANGE 10 and enhancing degradation efficiency. Conversely, when  $\text{pH} > \text{PZC}$ , the surface becomes negatively charged, leading to electrostatic repulsion that inhibits adsorption and lowers photocatalytic activity (C. Lee *et al.* 2023, L. Zhang *et al.* 2024, J. Díaz-Torres *et al.* 2022).

The main surface reactions can be expressed as:



Hydroxyl radicals ( $\cdot\text{OH}$ ) are generated by oxidation of water molecules trapped on the catalyst surface:



At very low pH, the adsorption of hydronium ions ( $\text{H}_3\text{O}^+$ ) on  $\text{TiO}_2$  reduces hydroxyl radical formation due to

competition for active sites, slightly lowering degradation efficiency. At high pH, excess hydroxide ions ( $\text{OH}^-$ ) can react with photogenerated holes, producing additional  $\cdot\text{OH}$  radicals, but excessive negative charge on the surface limits this effect (M. Jaafar *et al.* 2025).

The optimal degradation of ACID ORANGE 10 was achieved under mildly acidic conditions (around pH 6), consistent with trends reported for other anionic azo dyes (J. Díaz-Torres *et al.* 2022, M. R. Hoffmann *et al.* 2022, G. R. Peyton *et al.* 1974).

### 3.2.4. Effect of temperature

The photocatalytic degradation of ACID ORANGE 10 was studied at different temperatures (15, 25, and 35°C) under otherwise identical conditions.

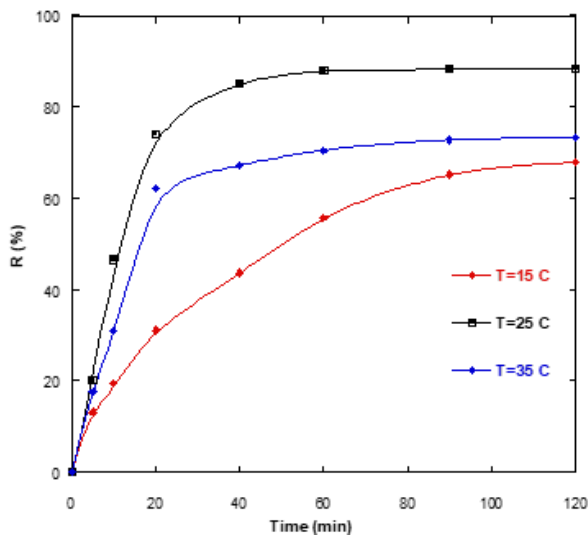


**Figure 11.** Effect of temperature on ACID ORANGE 10 degradation ( $[\text{ACID ORANGE 10}] = 10 \text{ mg L}^{-1}$ ;  $[\text{TiO}_2] = 0.1 \text{ g/L}$ ;  $V = 250 \text{ mL}$ )

As illustrated in **Figure 11**, temperature had a moderate effect on photocatalytic activity. The degradation efficiency increased from 67 % at 15°C to 88 % and 84 % at 25°C and 35°C, respectively. This indicates that the process is only weakly temperature-dependent within the investigated range.

At lower temperatures, the reduced degradation efficiency is mainly attributed to a decrease in dye adsorption on the  $\text{TiO}_2$  surface, which limits the formation of reactive hydroxyl radicals ( $\cdot\text{OH}$ ). The slight drop in activity observed at 35°C can be explained by the enhanced desorption of ACID ORANGE 10 molecules and faster recombination of photogenerated electron-hole pairs at elevated temperatures.

The temperature 25°C was identified as the most favorable operating temperature, providing a balance between sufficient adsorption of dye molecules and effective radical generation. Similar trends have been reported for other anionic dyes, confirming that photocatalytic degradation over  $\text{TiO}_2$  is primarily governed by photochemical rather than thermal activation (C. Lee *et al.* 2023, L. Zhang *et al.* 2024, J. Díaz-Torres *et al.* 2022).

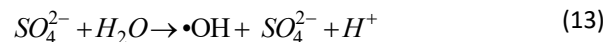
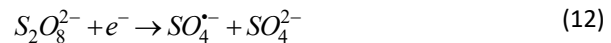
### 3.3. Process intensification by addition of oxidizing agents

Heterogeneous photocatalysis using  $\text{TiO}_2$  is an efficient approach for the degradation of organic pollutants. However, its performance can be further enhanced by coupling the UV/ $\text{TiO}_2$  system with external oxidizing substances such as persulfate ( $\text{S}_2\text{O}_8^{2-}$ ), hydrogen peroxide ( $\text{H}_2\text{O}_2$ ), hypochlorite ( $\text{Cl}^-/\text{HOCl}$ ), or iodate ( $\text{IO}_3^-$ ). These oxidants act as electron acceptors, suppressing charge recombination and can be reductively converted into highly reactive oxygen species (ROS) such as sulfate ( $\text{SO}_4^{2-}$ ), hydroxyl ( $\cdot\text{OH}$ ), chlorine ( $\text{Cl}^\bullet$ ), iodyl ( $\text{IO}_3^\bullet$ ) and periodyl ( $\text{IO}_4^\bullet$ ), and thereby improving degradation efficiency (S. Ahmed *et al.* 2010, T. Wu *et al.* 1998).

#### 3.3.1. UV/ $\text{TiO}_2/\text{K}_2\text{S}_2\text{O}_8$ system

Persulfate (PS) including potassium persulfate (KPS) has been investigated for wastewater remediation due to its capacity to degrade organic contaminants (I.A. Ike *et al.* 2028).

Persulfate ions ( $\text{S}_2\text{O}_8^{2-}$ ) are among the most powerful oxidants in aqueous solution. Upon UV activation, they produce sulfate radicals ( $\text{SO}_4^\bullet$ ) with higher redox potential ( $E^\circ = 2.6 \text{ V}$ ) and longer lifetime, and hydroxyl radicals ( $\cdot\text{OH}$ ) enabling efficient oxidation. Degradation mechanisms of sulfate radicals are based on hydrogen abstraction, addition on double bond and electron transfer, as shown in Equations (12-314):



The UV/ $\text{TiO}_2/\text{PS}$  results were compared with those obtained by UV/ $\text{TiO}_2$  and as expected, faster degradation was found at higher oxidant concentration. These radicals participate in hydrogen abstraction or electron-transfer reactions with organic compounds

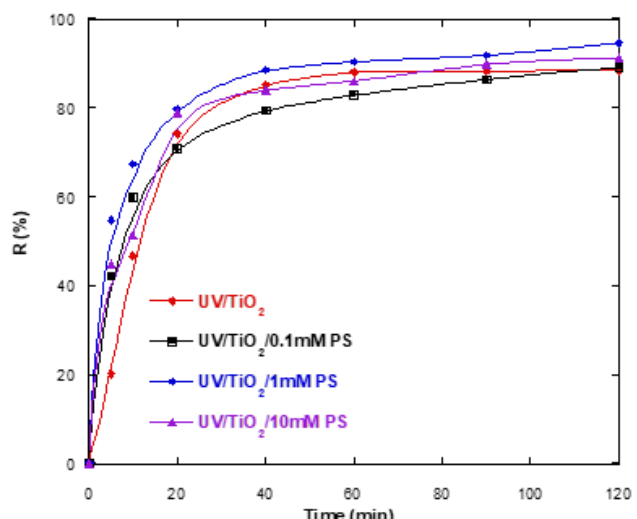


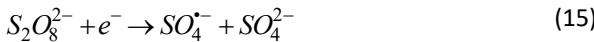
**Figure 12.** UV/ $\text{TiO}_2/\text{K}_2\text{S}_2\text{O}_8$  degradation system

**Figure 12** show the influence of persulfate dose on process efficiency. As illustrated, adding persulfate accelerated first ACID ORANGE 10 degradation compared

to UV/TiO<sub>2</sub> alone, and then decreased with the increasing persulfate dose. The improvement is attributed to both the inhibition of electron-hole recombination and the generation of SO<sub>4</sub><sup>•-</sup> radicals, which complement hydroxyl radicals in the oxidation process (F. Legrini *et al.* 1993).

The competitive destruction of the organic matter present in solution caused a slower dye abatement in the UV/TiO<sub>2</sub>/PS process, probably due to the larger attack of SO<sub>4</sub><sup>•-</sup> than •OH.

In contrast, when the persulfate dose was high ( $\geq 1\text{mM}$ ), no significant enhancement of removal efficiency was recorded, mostly due to the limited dosage of catalyst. However, when the excessive dosage of PS was introduced, the in situ generated SO<sub>4</sub><sup>•-</sup> radicals can be captured by persulfate molecules (Eq. (15)), thereby decreasing the decontamination efficiency (Y.R. Wang *et al.* 2019, P. L. Hao *et al.* 2020).



### 3.3.2. UV/TiO<sub>2</sub>/H<sub>2</sub>O<sub>2</sub> system

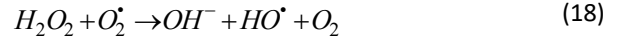
Hydrogen peroxide (H<sub>2</sub>O<sub>2</sub>) is a commonly used oxidizing substance ( $E^\circ = 0.8\text{ V}$ ), especially valued for producing hydroxyl radicals (•OH) under UV irradiation ( $\lambda < 330\text{ nm}$ ), in aqueous applications:



The addition of H<sub>2</sub>O<sub>2</sub> during UV/TiO<sub>2</sub> system treatment significantly improved the degradation efficiency. •OH generation increased substantially with higher H<sub>2</sub>O<sub>2</sub> doses at moderate concentrations (20 mM in this study), which enhances the degradation rate (Figure 13) by scavenging conduction-band electrons and promoting charge separation:



However, excessive H<sub>2</sub>O<sub>2</sub> may act as a radical scavenger, reducing efficiency through reactions [28-29] such as:



Therefore, using an optimal concentration is crucial for maximizing performance.

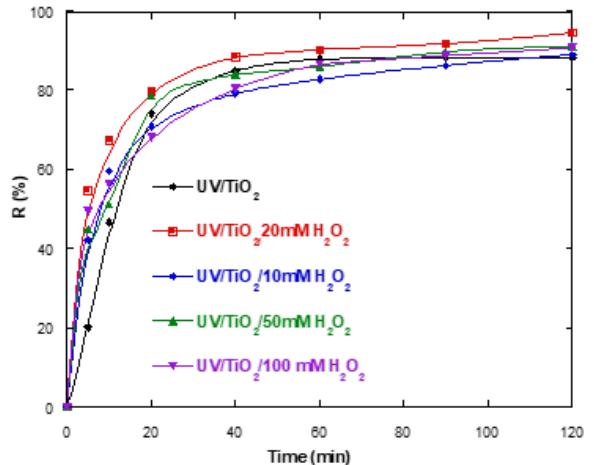


Figure 13. UV/TiO<sub>2</sub>/H<sub>2</sub>O<sub>2</sub> degradation system

### 3.3.3. UV/TiO<sub>2</sub>/Cl system

In advanced oxidation processes (AOPs), UV/Cl system is related to the synergistic UV-chlorination effects generating reactive species (RCS) such as Cl<sup>•</sup>, Cl<sub>2</sub><sup>•-</sup>, and ClO<sup>•</sup>. These radicals are characterized by greater redox potentials ( $E^\circ = 2.43\text{ V}$  for Cl<sup>•</sup>,  $E^\circ = 2.13\text{ V}$  for Cl<sub>2</sub><sup>•-</sup> and  $E^\circ = 1.5 - 1.8\text{ V}$  for ClO<sup>•</sup>), at environmentally pH values (pH 6–9).

In contrast to •OH, RCS are selective active species that can preferentially react with many rich electron organic compounds, these radicals are formed via photolysis (at 254 nm irradiation). Hypochlorous (HClO) forms •OH, Cl<sup>•</sup> radicals, and more reactive chlorine species during HClO photo-activation.

According to the following mechanism, multiple chemical reactions comprising several reactive radicals (Cl<sup>•</sup>, ClO<sup>•</sup>, •OH, O<sup>•</sup>, Cl<sub>2</sub><sup>•-</sup>) and non-radical intermediates/products (ClO<sup>-</sup>, Cl<sup>-</sup>) are described (Mohamed Larbi Djaballah *et al.* 2023):

**Figure 14** reflecting the synergistic effect of UV irradiation and chlorination. In this case, the free radical oxidation of ACID ORANGE 10 azo dye in chlorine photoactivated system was examine under different initial chlorine dosage (0,1-1 mM). During the UV/TiO<sub>2</sub>/Cl process, the initial concentration of ACID ORANGE 10 decreased rapidly, achieving up to 82% degradation within 5 min, higher than that of UV/TiO<sub>2</sub> alone (20%).

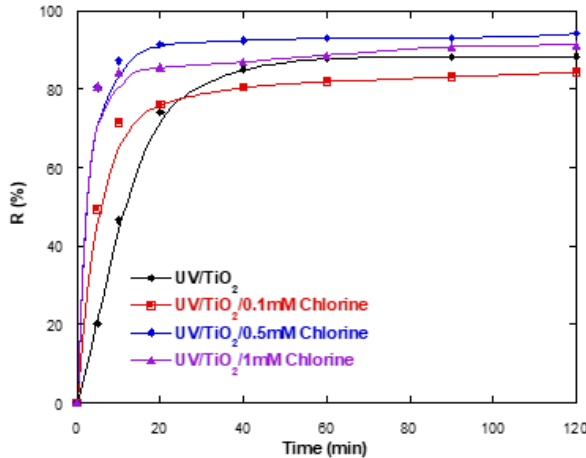


Figure 14. UV/TiO<sub>2</sub>/Cl degradation system

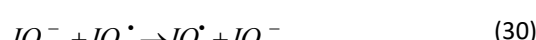
As HOCl absorbs 254nm photons, it photolyses into •OH and Cl<sup>•</sup>. These predominant reactants significantly improve the treatment efficiency.

When chlorine concentration exceeded 1mM, decline in dye degradation was observed and the generation of RCS entered a progressive inhibition stage. However, Cl<sup>-</sup> can scavenge •OH and Cl<sup>•</sup>, leading to the formation of dichlorine radical anion (Eq.13) which are regarded as being less reactive than Cl<sup>•</sup>. Therefore, although Cl<sup>-</sup> classified as a radicals-scavenger (J. Díaz-Torres *et al.* 2022).

### 3.3.4. UV/TiO<sub>2</sub>/IO<sub>3</sub><sup>-</sup> system

iodate is considered an economical oxidant due to its better chemical stability, easy storage, and transportation safety (Renxin Li *et al.* 2022). To improve the degradation performance of ACID ORANGE 10, a combination between photocatalysis and periodate (PI) activation processes was performed by adding potassium periodate, leading to the production of various oxidizing species like IO<sup>•</sup>, IO<sub>2</sub><sup>•</sup>, IO<sub>3</sub><sup>•</sup>, and •OH (M. L. Djaballah *et al.* 2021).

The different reactions occurring in a series of iodate photoactivation are represented as follows:



The above mechanism shows that, a negligible production of H<sub>2</sub>O<sub>2</sub> obtained from Eq.32, reflecting that H<sub>2</sub>O<sub>2</sub> have not

a significant role in the UV/IO<sub>3</sub><sup>-</sup> oxidation system (M. L. Djaballah *et al.* 2021). Consequently, iodine radical intermediates (IO<sup>•</sup>, IO<sub>2</sub><sup>•</sup>, IO<sub>3</sub><sup>•</sup>) are the dominants species in organic pollutants degradation.

The addition of iodate (IO<sub>3</sub><sup>-</sup>) significantly intensified the degradation process (Figure 15). Nearly complete ACID ORANGE 10 removal (~97%) was achieved within 120 min, compared to 82% without iodate. Consequently, this enhancement is due to the generation of iodine-based dominants radicals (IO<sup>•</sup>, IO<sub>2</sub><sup>•</sup>, IO<sub>3</sub><sup>•</sup>) under UV illumination. These radicals are highly reactive oxidizing species, synergistically promoting the breakdown of the aromatic structure of ACID ORANGE 10.

Recent studies confirm iodate radicals' high redox potential (N. Guettai *et al.* 2005). Moreover, iodate is characterized by its stability, storage and transport ability, and faster activation compared to other oxidants such as O<sub>3</sub>, H<sub>2</sub>O<sub>2</sub>, and persulfate (Y. Chen *et al.* 2023).

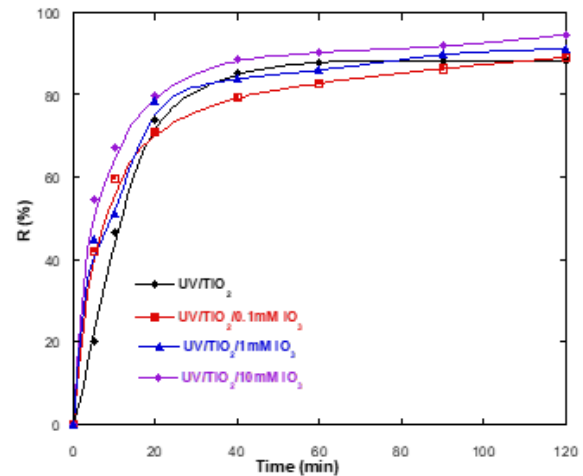


Figure 15. UV/TiO<sub>2</sub>/IO<sub>3</sub><sup>-</sup> degradation system

### 3.3.5. Comparative Study

As shown in Table 3, our optimized UV/TiO<sub>2</sub>/IO<sub>3</sub><sup>-</sup> system achieves superior performance (97% removal in 120 min) compared to literature reports for similar azo dyes under UV/TiO<sub>2</sub> systems (typically 60-80%). More remarkably, the combination of multiple oxidants (UV/TiO<sub>2</sub>/IO<sub>3</sub><sup>-</sup>/PS) achieves 97% removal in only 5 minutes, representing a 24-fold improvement in reaction rate compared to conventional UV/TiO<sub>2</sub>/H<sub>2</sub>O<sub>2</sub> systems. This enhanced performance is attributed to the synergistic generation of multiple reactive species (•OH, SO<sub>4</sub><sup>2-</sup>, IO<sub>3</sub><sup>•</sup>) that operate through complementary oxidation pathways."

### 3.3.6. Synergistic effect between oxidants

A comprehensive evaluation of ROS formation was achieved to determine the mechanism underlying the improvement in catalytic degradation compared to the ACID ORANGE 10 dye. When iodate, chlorine, persulfate and H<sub>2</sub>O<sub>2</sub>, entering into the system, promotes ROS generation, thereby enhancing the overall catalytic performance and confirm a strong synergistic effect between oxidants.

The observed acceleration of ACID ORANGE 10 degradation is mainly attributed to the generation of

multiple reactive radicals that interact synergistically to intensify oxidation.

The comparative studies in about the two radicals SO<sub>4</sub><sup>•-</sup> and •OH found that the degradation efficiency of ACID ORANGE 10 was higher by UV/PS (88%) than that in UV/H<sub>2</sub>O<sub>2</sub> (54%) in the first 5 min, which may attribute to

**Table 3.** Comparative performance of different photocatalytic systems for azo dye degradation

Study	Dye	System	Conditions	Removal (%)	Time (min)
This work	Acid Orange 10	UV/TiO <sub>2</sub> /IO <sub>3</sub> <sup>-</sup> , pH 6.5, 25°C		97	120
This work	Acid Orange 10	UV/TiO <sub>2</sub> /IO <sub>3</sub> <sup>-</sup> /PS, pH 6.5, 25°C		97	5
Lee <i>et al.</i> (2023)	Orange II	UV/TiO <sub>2</sub>	pH 3, 25°C	75	120
Zhang <i>et al.</i> (2024)	AO7		UV/TiO <sub>2</sub> /H <sub>2</sub> O <sub>2</sub> , pH 7, 30°C	68	90
Díaz-Torres <i>et al.</i> (2022)	RB5	UV/TiO <sub>2</sub> /PS	pH 5, 25°C	82	120

On the other hand, SO<sub>4</sub><sup>•-</sup> could also react with Cl<sup>-</sup> forming inorganic anion (Eq. 33), leading to the lower oxidation potential in UV/H<sub>2</sub>O<sub>2</sub> than that in UV/PS system.

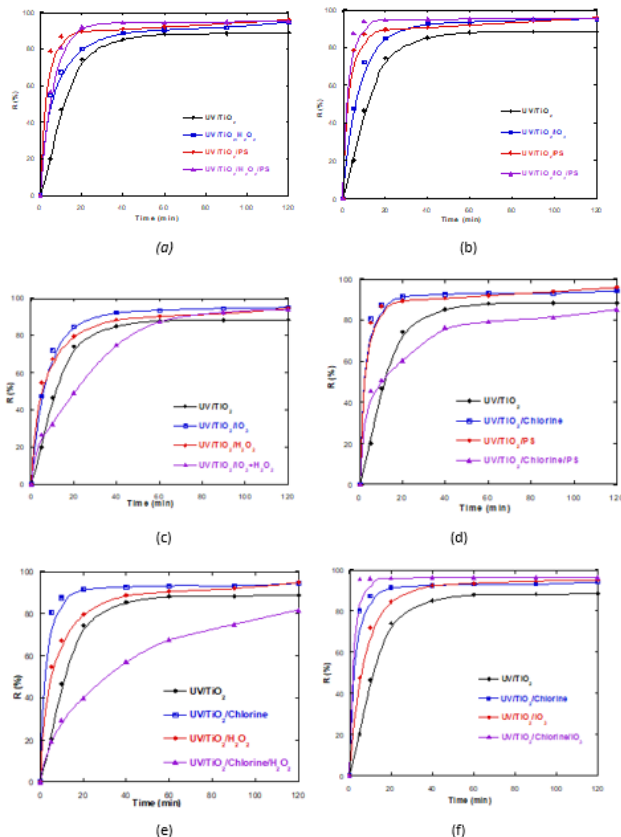
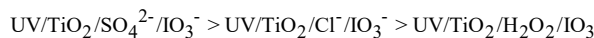


**Figure 16.** Comparative study of UV/TiO<sub>2</sub> degradation systems involving multiple oxidants: (a) PS/ H<sub>2</sub>O<sub>2</sub> , (b) PS/IO<sub>3</sub><sup>-</sup> , (c) IO<sub>3</sub><sup>-</sup> /H<sub>2</sub>O<sub>2</sub> , (d) PS/ Cl<sup>-</sup>, (e) Cl<sup>-</sup>/H<sub>2</sub>O<sub>2</sub>, (f) IO<sub>3</sub><sup>-</sup> / Cl<sup>-</sup>

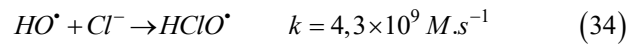
Conversely, the presence of iodine radical intermediates consistently improved performance across all hybrid systems, as expressed by the trend:



It should be noticed that this behavior confirms the beneficial role of iodine radicals (IO<sub>3</sub><sup>•</sup>, IO<sub>2</sub><sup>•</sup>, IO<sup>•</sup>) in sustaining electron transfer and reducing charge recombination.

the higher radical yield in UV/PS and stronger selectivity of SO<sub>4</sub><sup>•-</sup> than •OH. However, Hydroxyl radicals (•OH) have the shorter half-life with 20ns making it reacts rapidly, while the sulfate radicals are much lower (20–40 μs) (Hammouda S et al 2017) (Figure 16).

In contrast, the high values of residual H<sub>2</sub>O<sub>2</sub> harm the generation of HO<sup>•</sup> and Cl<sup>•</sup> in UV/Chlorine system (Eq.34) and rise HO<sup>•</sup> scavenging although producing the less reactive radical ClO<sup>•</sup>. Furthermore, the generation of highly reactive species which likely acted as competitors or scavengers for radicals generated during treatment limiting their availability in the solution (Figure 17).



The synergy factor (SI) was used to evaluate the degree of intensification, confirming that the combination of oxidants yields a non-linear enhancement greater than the sum of their individual effects. Nearly complete mineralization (~97%) was achieved in only 5min when all oxidizing species were present simultaneously.

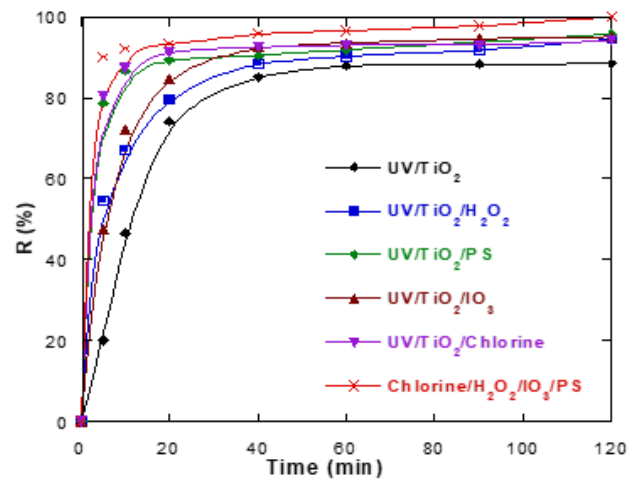


**Figure 17.** Roles of combined radicals in UV/TiO<sub>2</sub> system for ACID ORANGE 10 dye degradation

### 3.4. Photocatalytic degradation in semi-closed system

#### 3.4.1. Influence of inorganic and organic ions (MO and MNO)

In textile effluents, dyes are often accompanied by various inorganic and organic ions that can interfere with photocatalytic reactions. To evaluate this effect, different species such as KH<sub>2</sub>PO<sub>4</sub>, K<sub>4</sub>[Fe(CN)<sub>6</sub>], and CrK<sub>2</sub>O<sub>4</sub> were introduced into the UV/TiO<sub>2</sub> system at concentrations ranging from 0.1 to 2 mM (Figure 18).

The results show that at low concentrations, these ions have a negligible impact on degradation efficiency.

However, higher concentrations lead to a marked decrease in ACID ORANGE 10 removal due to the competitive adsorption and radical scavenging effects. Phosphate and chromate ions tend to adsorb onto the  $\text{TiO}_2$  surface, blocking active sites and altering the surface charge, while ferrocyanide complexes can act as electron donors, reducing the formation of reactive oxygen species (ROS).

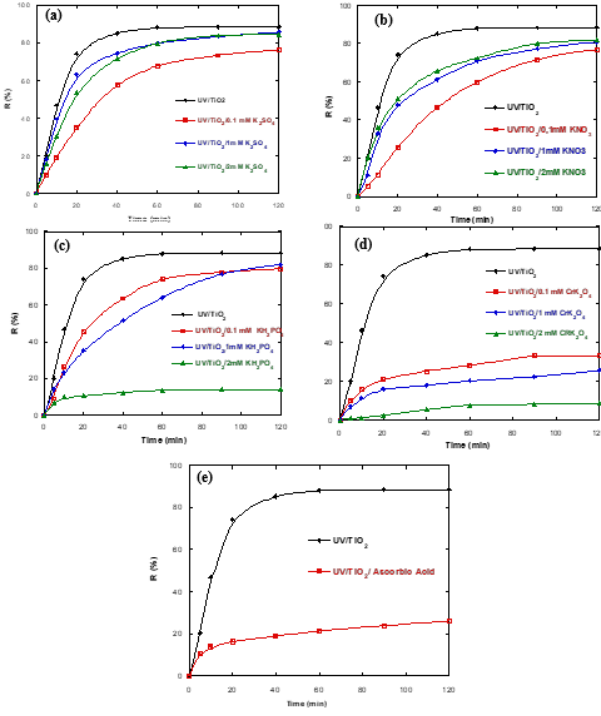


**Figure 18.** Effect of MO and MNO on the UV/TiO<sub>2</sub> degradation system. (a) UV/TiO<sub>2</sub>/K<sub>2</sub>SO<sub>4</sub>, (b) UV/TiO<sub>2</sub>/KNO<sub>3</sub>, (c) UV/TiO<sub>2</sub>/KH<sub>2</sub>PO<sub>4</sub>, (d) UV/TiO<sub>2</sub>/CrK<sub>2</sub>O<sub>4</sub>, (e) UV/TiO<sub>2</sub>/Ascorbic Acid

The presence of sulfate ions caused a moderate reduction in degradation rate, attributed to the formation of  $\text{SO}_4^{\bullet-}$  radicals that react more slowly with ACID ORANGE 10 than hydroxyl radicals. In contrast, nitrate ions exhibited a weak promoting effect through the following photolytic reactions:



$\text{NO}_2^{\bullet-}$  produced by nitrate photolysis. These secondary radicals slightly enhance oxidation, suggesting that nitrate-containing matrices can partially sustain photocatalytic activity under UV irradiation.

#### 3.4.2. Effect of alcohols

To identify the reactive species responsible for ACID ORANGE 10 degradation, alcohols such as ethanol, 2-propanol, and butanol were used as radical scavengers (Figure 19). These compounds selectively quench hydroxyl radicals ( $\bullet\text{OH}$ ) through hydrogen abstraction reactions, thereby reducing degradation efficiency.

The experimental results show a significant drop in removal efficiency from 88% (without scavenger) to 15-

40% depending on the type and concentration of alcohol. This strong inhibition confirms that  $\bullet\text{OH}$  radicals are the dominant oxidative species in the UV/TiO<sub>2</sub> system. Among the tested alcohols, butanol exhibited the highest quenching effect, consistent with its higher reactivity toward hydroxyl radicals (Peyton G.R *et al.* 1988, E. Vulliet *et al.* 2003).

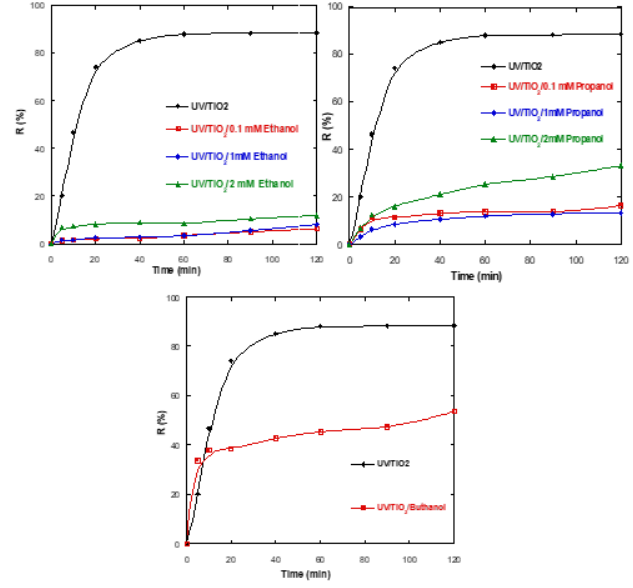


**Figure 19.** Influence of alcohols on the UV/TiO<sub>2</sub> system

#### 3.5. Effect of real water matrices

The complexity of real wastewater, due to dissolved salts, suspended solids, dissolved organic matter, and inorganic ions, can strongly influence photocatalytic efficiency. To assess the applicability of the developed process, ACID ORANGE 10 degradation was studied using four real matrices: distilled water, river water, seawater, and mineral water (Figure 20).

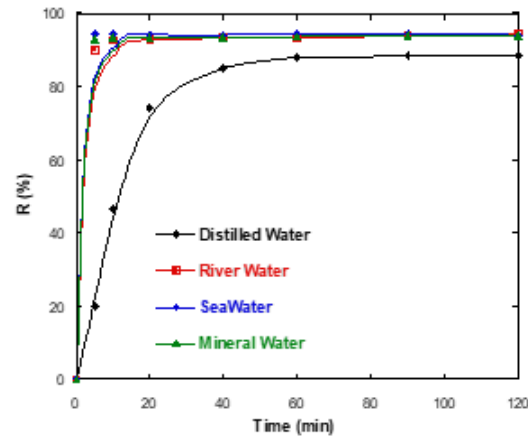


**Figure 20.** Effect of real matrices

The degradation performance remained high, achieving removal efficiencies of 94.5% (river water), 93.9% (seawater), and 93.6% (mineral water) within 5 min of treatment. The slight differences are attributed to the presence of natural ions (e.g.,  $\text{Na}^+$ ,  $\text{Mg}^{2+}$ ,  $\text{Cl}^-$ ,  $\text{SO}_4^{2-}$ ) that can compete for adsorption or scatter UV light. Nevertheless, the results demonstrate the robustness of

the UV/TiO<sub>2</sub> photocatalytic process for real aqueous matrices.

These findings validate the scalability of the process for industrial wastewater treatment, particularly for textile effluents containing azo dyes such as Acid Orange 10. The combination of optimized operational parameters and oxidant-assisted intensification confirms that the system can achieve efficient, rapid, and environmentally sustainable degradation.

### 3.6. Comparison with Hybrid Photocatalytic Systems

Recent advances in photocatalytic technology have explored various hybrid approaches combining photocatalysis with other treatment methods or modified catalysts. Our oxidant-assisted photocatalytic system can be positioned within this broader context of hybrid technologies.

**Catalyst modification approaches:** Studies have reported enhanced performance through TiO<sub>2</sub> modification including metal doping (Ag, Cu, Fe), non-metal doping (N, S, C), and composite formation (TiO<sub>2</sub>/graphene,

**Table 4.** Performance comparison with hybrid photocatalytic systems

System	Configuration	Removal (%)	Time (min)	Key advantage	Reference
This work	UV/TiO <sub>2</sub> /IO <sub>3</sub> <sup>-</sup> /PS	97	5	Simple operation	-
Modified catalyst	UV/N-TiO <sub>2</sub>	85	120	Visible light	(Nelson, K et al. 2024)
Photo-electro	UV/TiO <sub>2</sub> /Electric	90	60	Higher mineralization	(Machreki, M. et al., 2023)
Photo-membrane	UV/TiO <sub>2</sub> /UF	88	90	Continuous operation	(Bhattacharyya S et al., 2023)

Our results demonstrate that oxidant-assisted photocatalysis represents an effective and practical hybrid approach that balances performance, simplicity, and cost-effectiveness for industrial wastewater treatment applications.

## 4. Conclusion

This study demonstrates the efficiency of heterogeneous photocatalytic oxidation for degrading organic pollutants in wastewater, using Acid Orange 10 as a model contaminant. The UV/TiO<sub>2</sub> system effectively degraded the dye through hydroxyl radicals (•OH), following apparent first-order kinetics under optimized conditions (10 mg/L dye, 0.1 g/L catalyst, pH ≈ 6.5, 25°C).

Process intensification using external oxidants (persulfate, H<sub>2</sub>O<sub>2</sub>, iodate, chlorine) generated additional reactive species (SO<sub>4</sub><sup>2-</sup>, Cl<sup>•</sup>, IO<sub>3</sub><sup>•</sup>), achieving near-complete mineralization (~97%) with iodate showing the strongest synergistic effect. The system maintained high efficiency (>93%) in real water matrices (river, seawater, mineral water), confirming its applicability for complex industrial effluents.

Future work will focus on mechanistic investigations using EPR spectroscopy, development of visible-light-active catalysts, degradation pathway elucidation, ecotoxicological assessment, and pilot-scale validation under solar irradiation to enhance scalability and sustainability.

TiO<sub>2</sub>/carbon nanotubes). While these approaches improve visible light absorption and reduce electron-hole recombination, they typically require complex synthesis procedures and higher costs. In contrast, our approach of oxidant addition achieves comparable or superior performance enhancement (97% removal) using commercially available TiO<sub>2</sub> P25 and simple oxidant addition, offering practical advantages for industrial implementation (A, Rianjanu et al, 2024).

**Process coupling approaches:** Hybrid systems combining photocatalysis with electrochemical oxidation, membrane filtration, or biological treatment have shown promise. However, these approaches require multiple process units, complex equipment, and higher capital investment. Our semi-closed dual-reactor configuration with oxidant intensification achieves similar removal efficiencies with simpler equipment and operation.

**Comparative performance:** **Table 4** compares our system with recently reported hybrid approaches:

## References

Abha, S., Javed, A., & Faizan, S. J. S. (2018). Application of advanced oxidation processes and toxicity assessment of transformation products. *Environmental Research*, 167, 223-233.

Aditya Rianjanua, b, et al. (2024). Integrated adsorption and photocatalytic removal of methylene blue dye from aqueous solution by hierarchical Nb2O5@PAN/PVDF/ANO composite nanofibers. *Nano Materials Science*, 6, 96–105.

Ahmad, R., et al. (2016). Photocatalytic systems as an advanced environmental remediation: Recent developments. *Journal of Environmental Chemical Engineering*, 4, 4143-4164.

Ahmed, S., Rasul, M. G., Martens, W. N., Brown, R., & Hashib, M. A. (2010). Heterogeneous photocatalytic degradation of phenols in wastewater: A review on current status and developments. *Desalination*, 261, 3-18.

Ayad, D., et al. (2024). Sustainable water production study from simulation humid air by condensation unit. *Desalination and Water Treatment*, 320. 100885

Ayad, D., et al. (2025). Synthesis and characterization of a CNT/Fe2O3/TiO2/Bentonite nanocomposite for photocatalytic degradation of tetracycline hydrochloride. *Iranian Journal of Catalysis*, Volume 15, Issue 3, 152535 (1-11).

Bhattacharyya, S., Algieri, C., Davoli, M., et al. (2023). "Polymer-based TiO<sub>2</sub> membranes: An efficient route for recalcitrant dye degradation". *Chemical Engineering Research and Design*, 194, 589-602.

Brina, R., De Battisti, A. (1987). Electrochemical methods for teaching chemistry. *Journal of Chemical Education*, 64, 175-176.

Buxton, G. V., Sellers, R. M. (1985). Radiation-induced redox reactions of iodine species. *Journal of the Chemical Society, Faraday Transactions*, 81, 475-482.

Chen, Y., et al. (2023). Insights into periodate oxidation of antibiotics mediated by visible-light-induced polymeric carbon nitride: performance and mechanism. *Chemical Engineering Journal*, 457, 141147.

Dai, M., Niu, Q. Y., Wu, S. H., Lin, Y., Biswas, J. K., Yang, C. P. (2024). Hydroxyl radicals in ozone-based advanced oxidation of organic contaminants: a review. *Environmental Chemistry Letters*, 22, 3059-3106.

Díaz-Torres, J., et al. (2022). Photocatalytic oxidation of antibiotics using transition-metal-based systems. *Applied Catalysis B: Environmental*, 320, 121879.

Díaz-Torres, J., et al. (2022). Photocatalytic removal of emerging contaminants under visible light using modified catalysts. *Applied Catalysis B: Environmental*, 320, 121879.

Djaballah, M. L., Merouani, S., Bendjama, H., Hamdaoui, O. (2021). Development of a free radical-based kinetics model for the oxidative degradation of chlorazol black using periodate photoactivated process. *Journal of Photochemistry and Photobiology A*, 408, 113102.

El-Ghenemy, A., et al. (2022). Photocatalytic degradation of dyes using  $\text{TiO}_2$  nanomaterials. *Applied Catalysis B: Environmental*, 312, 121-139.

Furatian, L., Mohseni, M. (2018). Influence of chloride on the 185 nm advanced oxidation process. *Chemosphere*, 199, 1-8.

González-Labrada, K., et al. (2020). Enhancement of ciprofloxacin degradation by catalytic ozonation. *Environmental Science and Pollution Research*, 27, 1246-1255.

Guettai, N., Amar, H. A. (2005). Photocatalytic degradation of azo dyes. *Desalination*, 185, 427-438.

Guettai, N., Amar, H. A. (2005). Photocatalytic degradation of methyl orange in aqueous  $\text{TiO}_2$  suspension. *Desalination*, 185, 427-438.

Hammouda, S. B., et al. (2017). Degradation and mineralization of phenol in aqueous medium by heterogeneous monopersulfate activation on nanostructured cobalt-based perovskite catalysts  $\text{ACoO}_3$ . *Applied Catalysis B: Environmental*, 215, 60-73.

Hao, P. L., Hu, M. Z., Xing, R., Zhou, W. J. (2020). Synergistic degradation of methylparaben on  $\text{CuFe}_2\text{O}_4$ -rGO composite by persulfate activation. *Journal of Alloys and Compounds*, 823, 153757.

Hoffmann, M. R., Martin, S. T., Choi, W., & Bahnemann, D. W. (2022). Environmental applications of semiconductor photocatalysis. *Chemical Reviews*, 95, 69-96.

Ike, I. A., Linden, K. G., Orbella, J. D., & Duke, M. (2018). Critical review of the science and sustainability of persulphate advanced oxidation processes. *Chemical Engineering Journal*, 338, 651-669.

Karuppaiah, S., et al. (2019). Photocatalytic degradation of bisphenol A using  $\text{ZnO}$ /bentonite nanocomposite. *Applied Surface Science*, 481, 1109-1119.

Kumar, S., et al. (2023). "A review on photocatalysis used for wastewater treatment: dye degradation". *Water, Air, & Soil Pollution*, 234, 280.

Lee, C., et al. (2023). Degradation of organic pollutants using advanced oxidation processes: mechanisms and kinetics. *Journal of Environmental Chemical Engineering*, 11, 110807.

Legrini, O., Oliveros, E., & Braun, A. M. (1993). Photochemical processes for water treatment. *Chemical Reviews*, 93, 671-698.

Li, R., Wang, J., Han, W., Zhu, Z., & Guo, H. (2022). Periodate activation for degradation of organic contaminants: processes, performance and mechanism. *Separation and Purification Technology*, 292, 120928.

Li, S., et al. (2023). Antibiotics degradation by advanced oxidation process: ecotoxicity and antibiotic-resistance genes induction. *Chemosphere*, 311, 136977.

Lin, Y., Ferronato, C., Deng, N., Wu, F., Chovelon, J.-M. (2009). Photocatalytic degradation of methylparaben by  $\text{TiO}_2$ : multivariable experimental design and mechanism. *Applied Catalysis B: Environmental*, 88, 32-41.

Lu, Z., et al. (2022). Antibiotics degradation by UV/chlorine advanced oxidation processes: A comprehensive review. *Environmental Pollution*, 308, 119673.

Machreki, M., Chouki, T., Tyuliev, G., et al. (2023). "Defective  $\text{TiO}_2$  Nanotube Arrays for Efficient Photoelectrochemical Degradation of Organic Pollutants". *ACS Omega*, 8(15), 14066-14077.

Mohod, A. V., Teixeira, A. C. S. C., Bagal, M. V., Gogate, P. R., Giudici, R. (2023). Degradation of organic pollutants from wastewater using hydrodynamic cavitation: a review. *Journal of Environmental Chemical Engineering*, 11, 109773.

Mohammed J. A., et al. (2025). Effective adsorption of Chromium (III) ions from the tannery effluent wastewater using Cerium Oxide ( $\text{CeO}_2$ ) nanoparticles. *Indian Chemical Engineer*, Online, 1-18.

Nelson, K., Mecha, A.C., & Kumar, A. (2024). "Characterization of novel solar based nitrogen doped titanium dioxide photocatalytic membrane for wastewater treatment". *Heliyon*, 10(9), e29806.

Oller, I., Malato, S., & Sánchez-Pérez, J. A. (2011). Combination of advanced oxidation processes and biological treatments for wastewater decontamination: A review. *Science of the Total Environment*, 409, 4141-4166.

Peng, L., Yuan, Y., Wang, Z., Wang, W., & Wu, Q. (2024). Iron single atoms anchored on ultrathin carbon nitride photocatalyst for visible-light water decontamination. *Journal of Hazardous Materials*, 474, 134703.

Peyton, G. R., & Glaze, W. H. (1988). Destruction of pollutants with ozone/UV: photolysis of aqueous ozone. *Environmental Science & Technology*, 22, 761-767.

Rook, J. J. (1974). Formation of haloforms during chlorination of natural waters. *Water Treatment and Examination*, 23, 234-241.

Samadi, M., Zirak, M., Naseri, A., Khorashadizade, E., & Moshfegh, A. Z. (2016). Fabrication and characterization of  $\text{ZnO}$  nanostructures for photocatalytic applications. *Thin Solid Films*, 605, 19-26.

Sivasubramanian S, Gopalsamy Venkatesan SK, Thanarajan T, Rajendran S. (2025). Al-Biruni Earth Radius Optimization for enhanced environmental data analysis in remote sensing imagery. *Agrociencia*. Vol 59i5.3380.

Sleiman, M., Conchon, P., Ferronato, C., & Chovelon, J.-M. (2009). Photocatalytic oxidation of toluene at indoor air levels. *Applied Catalysis B: Environmental*, 86, 159-165.

Suty, H., de Traversay, C., Coste, M. (2021). Application of AOPs: Present and future. *Water Science and Technology*, 8, 12-23.

Venkatraman M., Surendran R., Srinivasulu S., Vijayakumar K. (2024). Water quality prediction and classification using Attention based Deep Differential Recur Flow Net with Logistic Giant Armadillo Optimization", *Global NEST*, Vol 27, No 1, 06799.

Vulliet, E., Chovelon, J.-M., Guillard, C., & Herrmann, J.-M. (2003). Factors influencing the photocatalytic degradation of sulfonylurea herbicides by  $TiO_2$ . *Journal of Photochemistry and Photobiology A*, 159, 71-79.

Wang, Y. R., et al. (2019). Nanoscaled magnetic  $CuFe_2O_4$  as an activator of PMS for norfloxacin degradation. *Separation and Purification Technology*, 212, 536-544.

Wang, H. J., et al. (2025). Controlled construction of single-atom iron for pollutant elimination. *Chemical Engineering Journal*, 516, 164113.

Wu, T., Liu, G., Zhao, J., Hidaka, H., Serpone, N. (1998). Self-photosensitized oxidative transformation of Rhodamine B. *Journal of Physical Chemistry B*, 102, 5845-5851.

Yang, Q., et al. (2019). Recent advances in photo-activated sulfate radical-AOP for refractory organic pollutants. *Chemical Engineering Journal*, 378, 122149.

Yudha Gusti Wibowoa, et al. (2025). Biochar-layered double hydroxide vs biochar-layered double oxide: a critical review on their applications in water pollution control. *Water-Energy Nexus*, 8, 205-228

Zadvarzi, S. B., Khavarpour, M., Vahdat, S. M., Baghbanian, S. M., & Rad, A. S. (2021).  $Fe_3O_4@chitosan@ZIF-8$  for removal of malachite green. *International Journal of Biological Macromolecules*, 168, 428-441.

Zaviska, F., Drogui, P., Mercier, G., Blais, J. (2009). Advanced oxidation processes in water treatment: A review. *Environmental Technology*, 30, 1101-1110.

Zhang, L., et al. (2024). Degradation of dyes in aqueous media via sulfate radical AOP. *Chemosphere*, 352, 140221.

Zhang, X., Duan, X., Sun, H., Wang, S. (2019). Activation of persulfate by transition metals for organic pollutant degradation. *Chemical Engineering Journal*, 370, 1167-1180.

Zhang, X., Yu, X., Kamali, M., Appels, L., Van der Bruggen, B., Cabooter, D., Dewil, R. (2021). Efficiency and mechanism of 2,4-dichlorophenol degradation by UV/ $IO_4^-$ . *Science of the Total Environment*, 782, 146781.

Zhao, Y., et al. (2020). Scavenging of pharmaceuticals by activated carbon fiber. *Chemosphere*, 247, 1259.

Zhu, Z., Zhao, X., Xiao, X., Xu, C., Zuo, X., Nan, J. (2022). Formation of surface oxygen vacancies in Bi-based hybrid photocatalyst. *Journal of Colloid and Interface Science*, 625, 109-118.